COBEM 2025
28TH INTERNATIONAL CONGRESS OF MECHANICAL ENGINEERING
ABCM Brazilian Society of Mechanical Sciences and Engineering
28th ABCM International Congress of Mechanical Engineering
November 09-11, 2025, Curitiba-PR, Brazil

COB-2025-0583

NUMERICAL MODELING OF THE EFFECT OF MASS FLOW RATE ON THE INTERNAL TEMPERATURE OF THE CYCLONE

Mateus Filipe Ribeiro Silva
Paloma Martins de Meira
Fábio Santos Nascimento
Carlos Eymel Campos Rodriguez
Rubén Allexis Carrillo
Rogério Fernandes Brito
Federal University of Itajubá, UNIFEI, Theodomiro Carneiro Santiago Campus – Itabira, Irmã Ivone Drumond, St. #200 – Distrito Industrial II, Zip code: 35,903-087, Itabira – MG – Brazil.
mateusfilipesilva@gmail.com, palomameira464@gmail.com, fabiosn@unifei.edu.br, carloscampos@unifei.edu.br, ruben,miranda@unifei.edu.br, rogbrito@unifei.edu.br

Abstract. This study was undertaken for performing numerical simulation of the drying sugarcane bagasse with variations in the mass flow rates of the incoming particles. Bagasse is one of the main raw materials available for combustion supply to the power plants and needs drying. The author utilized the RNG k-ε turbulence model and an Eulerian-Lagrangian methodology for multiphase transport; cyclone geometry was analyzed in SolidWorks; the cases studied were meshed in ICEM CFD and ANSYS CFX; the mass flow rates investigated were 9.5 g/s and 16 g/s. Cyclone temperature varies inversely with the mass flow rate; lower flow rates provide hotter cyclones. The underflow outlet temperature is 267 ºC, whereas the upper-outlet temperature is 273 ºC for 9.5 g/s, whereas they become closer for 16 g/s, according to Table 1. The results above demonstrate the requirements for mass flow optimization in dry sugarcane bagasse industrial applications.

Keywords: *Sugarcane bagasse, Drying efficiency, CFD simulation, Cyclone separator, Mass flow rate*

1. INTRODUCTION

The escalating demand for renewable energy sources has propelled the utilization of sugarcane bagasse as a solid biomass for heat and electricity generation. Brazil, as the world's largest sugarcane producer, annually processes over 637 million tons (CONAB, 2023), resulting in a substantial volume of lignocellulosic residue. However, the high moisture content of bagasse, typically ranging from 45% to 55% on a wet basis, diminishes its energy efficiency when used directly as fuel. According to Bahadori *et al.* (2014), reducing bagasse moisture content is directly correlated with enhancing the thermal efficiency of industrial boilers. Addressing this challenge necessitates a deeper understanding of the complex drying processes involved, which can be effectively explored through advanced modeling techniques such as Computational Fluid Dynamics (CFD).

Computational simulation, particularly CFD, enables the visualization of phenomena that are difficult to observe experimentally, such as the formation of recirculation zones, the presence of internal thermal gradients, and the dynamic behavior of particles. Turbulence models such as RNG k-ε are widely employed to represent the rotational flow typical of cyclones (Azadi *et al.*, 2010), while the interaction between the gas and solid phases is described using the Eulerian–Lagrangian approach (Safikhani *et al.*, 2021).

Scientific literature demonstrates that the particle mass flow rate exerts a critical influence on the thermal performance of cyclone dryers. Elevated flow rates significantly reduce the residence time of particles within the equipment, which limits heat transfer and, consequently, drying efficiency. A numerical study conducted by Siadaty *et al.* (2017), utilizing ANSYS Fluent software, demonstrated that doubling the inlet flow rate decreased the average particle residence time by up to 35%, with a direct impact on separation efficiency and moisture removal. Conversely *et al.* (2024), applying Large Eddy Simulation (LES), observed that lower flow rates promote greater vortex core stability and elevate the average temperature in the cyclone's drying zone, favoring the moisture evaporation process and increasing the system's thermal yield.

Recent studies demonstrate that temperature behavior within cyclones is strongly influenced by internal flow structures, especially the Precessing Vortex Core (PVC). In an investigation conducted by Brar and Rahmani (2024), utilizing numerical simulation with the Large Eddy Simulation (LES) model, it was observed that the PVC forms at the center of the cyclone as an oscillatory rotating region and causes temperature and pressure fluctuations that reduce the system's thermal stability. The study by Dong *et al.* (2020) evaluated vortex eccentricity and showed that perturbations

in the vortex core can compromise thermal efficiency and drying uniformity. Furthermore, Yuan *et al.* (2024) explored the impact of the short-circuit flow rate – a gas flow that directly traverses the cyclone from inlet to outlet without participating in separation – and identified that its control is essential to prevent heat losses and ensure better thermal distribution within the equipment.

Additionally, geometric modifications in cyclones have been widely studied with the aim of improving separation efficiency and thermal performance in processes involving suspended particles. He *et al.* (2025) numerically investigated the effect of inserting a secondary vortex finder (SVF) in cyclones arranged in series. The results of the CFD simulation showed that this modification contributed to reducing kinetic energy losses and smoothing the secondary flow, increasing the overall separation efficiency of the system by more than 12%. Conversely, Yohana *et al.* (2022) evaluated the effects of a modified conical vortex finder geometry and external cooling of the cyclone body. The authors concluded that these interventions improved the uniformity of the velocity field and decreased wall temperatures, which contributes to greater thermal stability and improved drying process efficiency.

In the Brazilian scenario, although studies involving CFD modeling in cyclonic dryers focused on biomass are still limited, some relevant investigations have demonstrated the applicability of this technique for thermal optimization. An example is the work by Gupta *et al.* (2022), who applied numerical simulation with ANSYS CFX software to model the performance of thermal systems involving biomass, evaluating parameters such as temperature distribution and energy efficiency. The study reinforces that the use of adapted geometries, combined with CFD, can reduce thermal losses and improve the utilization of available energy. Despite its global focus, the authors highlight the applicability of the tools for agricultural and industrial contexts in countries with large biomass production, such as Brazil.

Beyond fluid-thermal modeling in cyclones, complementary studies have reinforced the importance of Computational Fluid Dynamics (CFD) in other forms of thermal utilization of sugarcane bagasse, such as gasification and combustion in fluidized beds. Centeno-González *et al.* (2017) utilized CFD simulations to analyze the behavior of bagasse during combustion in industrial boilers. The validated model allowed for precise estimation of temperature profiles and gas concentrations along the burner, contributing to the energy optimization of the process. Medeiros *et al.* (2020) conducted numerical modeling of bagasse gasification in a fast fluidized bed, observing that the combination of optimized operational conditions and validation by experimental data ensured good agreement between simulation and reality, indicating the technique's potential to predict thermal performance in complex systems.

Thus, the numerical study of sugarcane bagasse drying with varying inlet mass flow rates directly contributes to the optimization of industrial processes. The knowledge generated from these simulations allows not only for operational improvements but also for the development of more efficient and sustainable equipment, aligned with the country's environmental and energy commitments.

2. METHODOLOGY

2.1 DESCRIPTION OF THE ANALIZED CASE

The present study investigates the influence of particle mass flow rate on the internal thermal behavior of a cyclone dryer used for sugarcane bagasse. To establish a solid foundation for comparison, the study by Silva (2016) was revisited. In that work, simulations were conducted using a cyclone geometry originally proposed by Corrêa (2003), with variations in key inlet parameters such as particle mass flow rate, air velocity, air temperature, and moisture content.

This approach allows the current work to expand the understanding of the system's behavior by simulating two new mass flow rate cases (9.5 g/s and 16 g/s), which were selected to fall between the previously studied values. These cases provide additional insights into the thermal dynamics of bagasse drying under varying loading conditions, aiming to support process optimization efforts in industrial biomass applications.

It is also worth noting that there are some differences between the images used for validation and those from the present work. This discrepancy may be attributed to the fact that, although the mathematical modeling was the same, several parameters inherent to the CFX configuration were not available—such as certain items related to the boundary conditions for walls and inlet/outlet regions. Therefore, the absence influenced the graphical representation of the results in CFX-Post.

2.2 GEOMETRY AND COMPUTATIONAL MESH

The cyclone geometry used in this study is the same as that employed by Silva (2016), and was modeled using SolidWorks software with the dimensions shown in Figure 1.

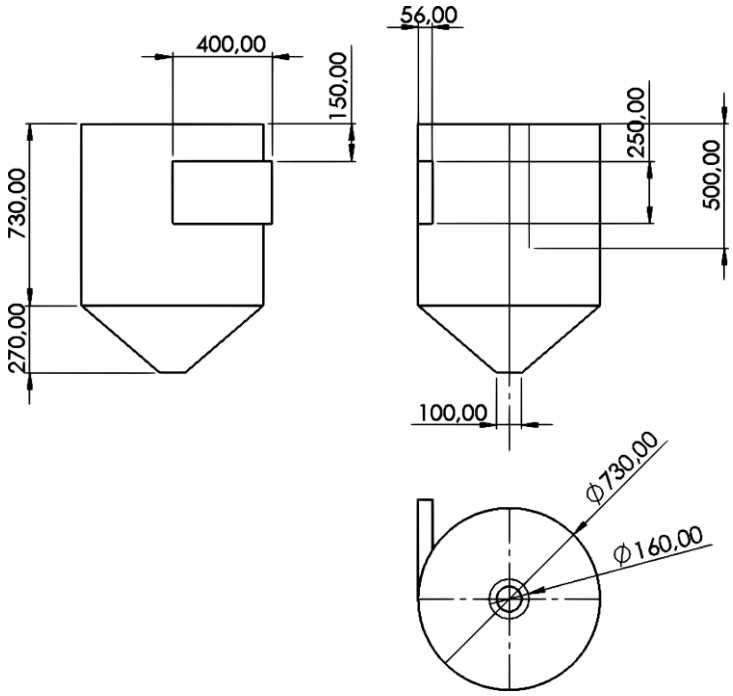

Figure 1. Geometry used for the simulations [mm]. (Source: Adapted from Silva, 2016)

Subsequently, the ICEM CFD package from ANSYS was used to generate the representative mesh of the cyclone using the blocking strategy, which subdivides the solid into several blocks to produce a refined mesh. The mesh employed in the present study consists of 250,000 hexahedral elements, ensuring that it does not interfere with the results, and is shown in Figure 2.

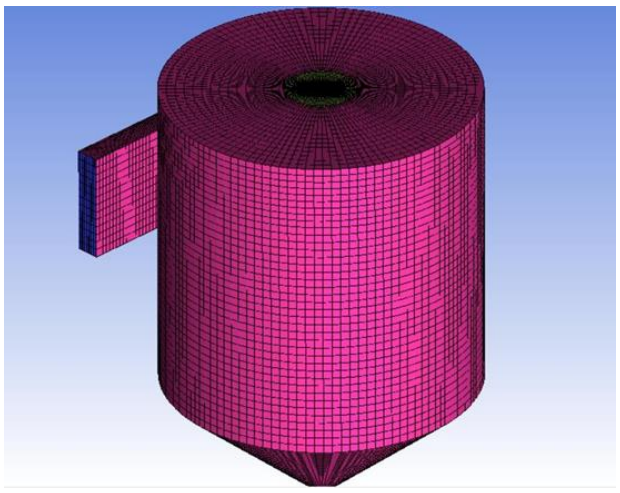

Figure 2. Computational mesh.

2.3 MATHEMATICAL AND NUMERICAL MODELINGG

The numerical simulations adopted an Eulerian–Lagrangian multiphase approach.

The gas phase (air) was modeled using the continuity, momentum (Navier–Stokes), and energy equations, while the particle phase (sugarcane bagasse) was modeled as discrete entities subject to Newton's second law.

The turbulence model selected was RNG k-ε, suitable for swirling and recirculating flows in cyclone-type devices.

The following assumptions were made:

- Steady-state flow;
- Constant fluid properties;
- Influence of gravity included;
- Particles composed entirely of water;

- No chemical reactions.

2.3.1 GAS PHASE MODEL

The main equations used were:

- Continuity, Eq. (1):

$$\nabla \cdot (\boldsymbol{\rho}\vec{\boldsymbol{u}}) = 0 \tag{1}$$

where $\boldsymbol{\rho}$ and $\vec{\boldsymbol{u}}$ are continuous phase density and velocity vector.

- Momentum, Eq. (2):

$$\nabla \cdot (\boldsymbol{\rho}\vec{\boldsymbol{u}}\vec{\boldsymbol{u}}) = -\nabla \boldsymbol{p} + \nabla \cdot \boldsymbol{\tau} + \boldsymbol{S}_{\mathrm{m}} \tag{2}$$

where $\mathbf{p}, \boldsymbol{\tau}$ and $\boldsymbol{S_m}$ are pressure, shear stress and source term.

- Energy, Eq. (3):

$$\nabla \cdot (\boldsymbol{\rho}\vec{\boldsymbol{u}}\boldsymbol{h_0}) = \nabla \cdot (\boldsymbol{\lambda}\boldsymbol{\nabla T}) + \nabla \cdot (\vec{\boldsymbol{u}} \cdot \boldsymbol{\tau}) \tag{3}$$

where $\boldsymbol{h_0}$, $\boldsymbol{\lambda}$ and $\boldsymbol{T}$ are stagnation enthalpy, thermal conductivity and absolute temperature.

2.3.2 PARTICLE PHASE (SUGARCANE BAGASSE) MODEL

Equation (4) represents the interaction between the fluid phase and the particulate phase is given by Newton's 2nd Law, where $\vec{\boldsymbol{F}}$ corresponds to the summation of drag forces acting on the particles.

$$\vec{\boldsymbol{F}} = \frac{1}{8}\pi \boldsymbol{d}^2 \widehat{\boldsymbol{f_s}} \boldsymbol{\rho} \boldsymbol{C_D} \left|\overrightarrow{\boldsymbol{V_r}}\right| \overrightarrow{\boldsymbol{V_r}} \tag{4}$$

where $\mathbf{d}$, $\widehat{\boldsymbol{f_s}}$, $\boldsymbol{C_D}$ and $\overrightarrow{\boldsymbol{V_r}}$ represents the particle diameter, cross-sectional area factor, drag coefficient defined by the Ishii/Zuber correlation and relative particle-gas velocity, respectively.

The drag force between fluid and particles followed the Ishii–Zuber correlation with geometric corrections. The Ishii/Zuber correlation is generally applied to spherical particles, requiring correction for non-spherical particle geometries, as is the case for sugarcane bagasse particles. In this study, two correction factors were used, Eqs (5) or (6):

$$\widehat{\boldsymbol{f_s}} = \frac{\boldsymbol{A_{ne}}}{\boldsymbol{A_e}} \tag{5}$$

where $\boldsymbol{A_{ne}}$ and $\boldsymbol{A_e}$ are the cross-sectional area of a non-spherical particle with volume V and cross-sectional area of a spherical particle with volume. The other factor that can been used is:

$$\widehat{\boldsymbol{f_s}} = \frac{\boldsymbol{S_e}}{\boldsymbol{S_{ne}}} \tag{6}$$

where $\boldsymbol{S_e}$ and $\boldsymbol{S_{ne}}$ denote the surface area of a spherical particle with volume V and surface area of a spherical particle with volume V.

This relationship is valid for particle Reynolds numbers between 0.2 and 1000.

2.3.3 HEAT TRANSFER BY CONVECTION

Convective heat transfer was modeled using the Ranz–Marshall correlation in Eq. (7):

$$\mathbf{Nu} = 2 + 0{\cdot}6\mathbf{Re_p^{0{\cdot}5}Pr^{0{\cdot}33}} \tag{7}$$

where **Nu**, **Re**, and **Pr** represent the dimensionless numbers.

This relation holds for particle Reynolds numbers below 5×10^7 and Prandtl numbers in the range of 0.5 to 2000

2.3.4 LATENT HEAT TRANSFER IS ASSOCIATES WITH MASS TRANSFER

The energy used to evaporate water on the particle surface, $\boldsymbol{Q_m}$, is the sum of the energy of each particle entering the cyclone, as shown in Eq. (8).

$$\boldsymbol{Q_m} = \sum \frac{\boldsymbol{dm_p}}{\boldsymbol{dt}} \boldsymbol{h_{fg}} \tag{8}$$

where $\frac{\boldsymbol{dm_p}}{\boldsymbol{dt}}$ and $\boldsymbol{h_{fg}}$ are difined as mass transfer between the particles and fluid, and the latent heat of vaporization, which is a function of temperature, respectively.

This model is valid for mass or heat transfer Biot numbers less than 0.1, where conduction is faster than convection.

Mass transfer between the particles and the fluid is determined by the Eq. (9):

$$\frac{\boldsymbol{dm_p}}{\boldsymbol{dt}} = \pi \boldsymbol{d_p \rho D Sh} \frac{\boldsymbol{PM_v}}{\boldsymbol{PM_g}} log\left(\frac{1-\boldsymbol{X_e}}{1-\boldsymbol{X_g}}\right) \tag{9}$$

in which ***D***, ***PMv***, ***PMg***, ***Xe***, ***Xg***, and ***Sh*** represent the dynamic diffusivity; molecular weight of water vapor; molecular weight of the gas; equilibrium mole fraction; gas mole fraction and Sherwood number respectively.

Sherwood number Eq. (10) represents the ratio between convective and diffusive mass transfer.

$$\boldsymbol{Sh} = 2 + 0.6 \boldsymbol{Re_p^{\frac{1}{2}} Sc^{\frac{1}{3}}} \tag{10}$$

This relationship is valid for particle Reynolds numbers between 2 and 200.

Schmidt number, **Sc**, is defined by Eq. (11):

$$\boldsymbol{Sc} = \frac{\boldsymbol{\mu}}{\boldsymbol{\rho D_{ag}}} \tag{11}$$

where $\boldsymbol{\mu}$ is the dynamic viscosity of the fluid phase.

Equation (12) is applied when the particle temperature is below the bubble point; otherwise, the following equation is used:

$$\frac{\boldsymbol{dm_p}}{\boldsymbol{dt}} = -\frac{\boldsymbol{Q_c}}{\boldsymbol{Q_m}} \tag{12}$$

Here $\frac{\boldsymbol{dm_p}}{\boldsymbol{dt}}$, $\boldsymbol{Q_c}$, and $\boldsymbol{Q_m}$ are the mass transfer rate, convective heat transfer, and the amount of latent heat due to vaporization.

The vapor pressure is determined using the Antoine equation, given by Eq. (13):

$$\boldsymbol{P_{vapor}} = \boldsymbol{P_{ref}} e^{\left(\boldsymbol{A} - \frac{\boldsymbol{B}}{\boldsymbol{C+T}}\right)} \tag{13}$$

where *A*, *B*, and *C* are models constants.

Simulations were performed using ANSYS CFX, with a convergence criterion of residuals < 1×10^{-4}.

2.4 BOUNDARY CONDITION

2.4.1. CYCLONE WALLS

The no-slip condition was adopted, meaning that the velocity at the walls is zero, as expressed in Eq. (14):

$$\mathbf{U_X} = \mathbf{U_y} = \mathbf{U_Z} = 0 \tag{14}$$

The heat flux was assumed to be adiabatic, i.e., the cyclone walls do not exchange heat with the external environment, as shown in Eq. (15).

$$\mathbf{Qwalls} = 0 \tag{15}$$

2.4.2. CYCLONE OUTLET SECTION

The pressure was set equal to atmospheric pressure, as defined in Eq. (16).

$$\mathbf{P} = \mathbf{P_{atm}} \tag{16}$$

The Neumann boundary condition for temperature was applied, meaning that the temperature does not vary in the direction normal to the boundary, as shown in Eq. (17).

$$\frac{dT}{dy} = 0 \tag{17}$$

2.4.3. PARAMETERS USED

Table 1 presents the defined property values of the materials used in the drying process of sugarcane bagasse, namely air at 25 °C and the bagasse particles. During the simulation, the particle was assumed to be composed entirely of water in order to simplify the drying model.

Table 1. Values used in the simulation

Properties	Fluid (air at 25 °C)	Particle (sugarcane bagasse)
Density (kg/m³)	1.185	958.37
Thermal conductivity (W/m·K)	3.7673×10^{-2}	0.215
Latent heat of vaporization (J/kg)	-	2.251×10^{6}
Diffusivity (m²/s)	4.0787×10^{-5}	-
Molecular weight (kg/kmol)	28.96	18.02
Particle diameter (mm)	-	6.35
Particle temperature (ºC)	-	30.6
Surface area factor	-	2.18
Cross-sectional area factor	-	3.89

2.4.4. OBJECTIVE

The objective of the present study is to investigate the influence of varying particle mass flow rate on the drying process. An air inlet velocity of 15 m/s and a temperature of 277 °C were selected, as these values produced the best results in the simulations conducted by Silva (2016). The particle mass flow rates, in turn, were selected to fall between the values used by Silva (2016), specifically 9.5 g/s (Case 1) and 16 g/s (Case 2), in order to expand the scope of the study on mass flow variation in the particle inlet of cyclone dryers.

3. RESULTS AND DISCUSSION

This section discusses the results of two cases simulated using ANSYS CFX, varying the particle inlet mass flow rate with values of 9.5 g/s and 16 g/s.

Figure 3 illustrates the internal temperature profiles obtained from Silva's cyclone (2016) in cases where the particle inlet mass flow rate was varied, which is the main objective of the present study. Figures 3a, 3b, and 3c illustrate mass flow rates of 6 g/s, 13.1 g/s, and 19.5 g/s, respectively. It can be observed that as the mass flow rate increases, the internal temperature of the cyclone decreases, especially in the lower conical section of the cyclone.

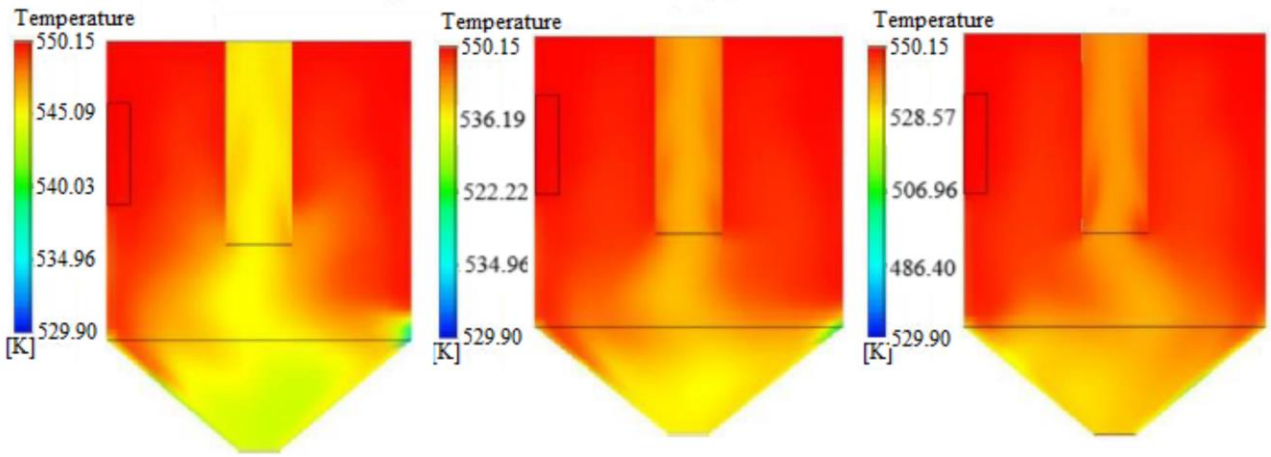

Figure 3. Internal temperature profile of the cyclone for different mass flow rates: a) 6.55 g/s, b) 13.1 g/s, and c) 19.65 g/s (Source: Silva, 2016).

Figure 4 presents the temperature contour plot in the central interior of the cyclone for both particle mass flow rates. It can be observed that for both cases, the regions with the lowest temperatures are the conical region and the central duct region. This occurs because these areas represent the outlets, where both particles and hot air exit after exchanging heat. For the case with a mass flow rate of 9.5 g/s, the inlet temperature is 277 ºC, while the bottom outlet temperature is approximately 267 ºC and the top outlet temperature is 273 ºC. Conversely, for the 16 g/s mass flow rate case, the inlet temperature is also 277 ºC, but the bottom outlet temperature is approximately 261 ºC, and the top outlet temperature is 269 ºC. A comparison of these values reveals that the internal cyclone temperature reaches lower values when the particle mass flow rate is higher.

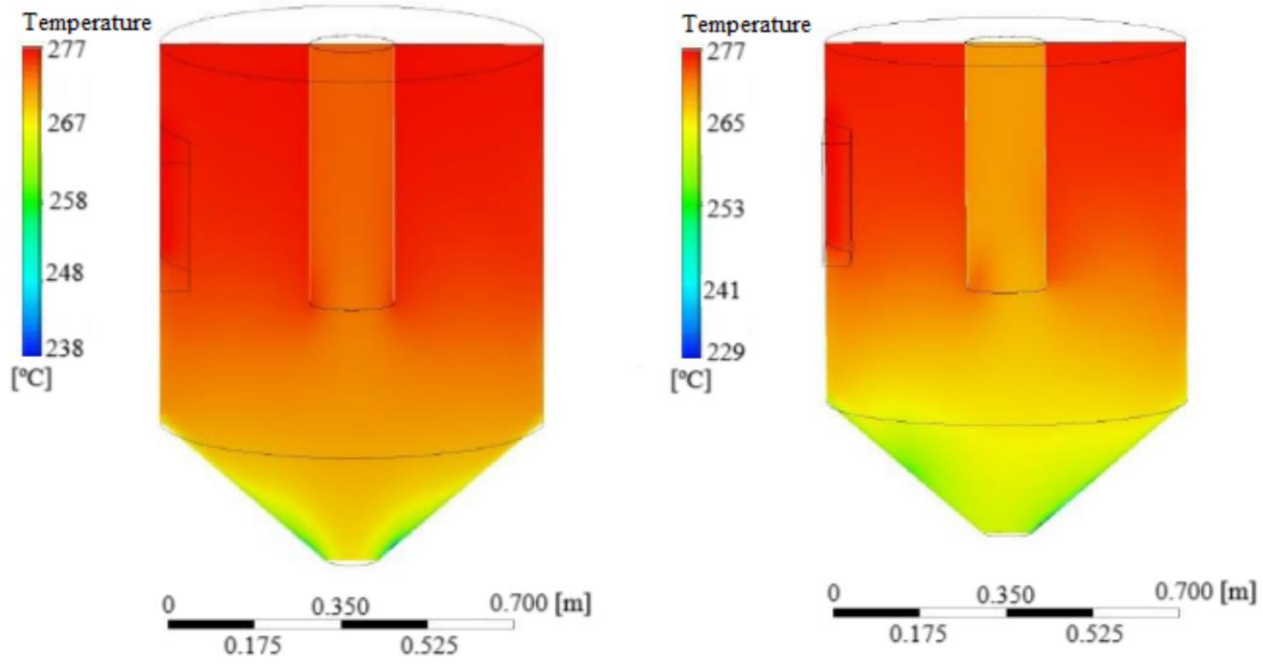

Figure 4. Internal temperature profile of the cyclone for mass flow rates of 9.5 and 16 g/s, respectively.

An explanation for this phenomenon is that a higher mass flow rate results in an increased heat exchange between the air and the particles, due to the larger contact surface area between the two phases. This enhanced interaction leads to a reduction in the overall internal temperature of the cyclone. The internal temperature distributions align with the trend observed in Figure 3, confirming that the mass flow rate is inversely proportional to the internal temperature of the cyclone.

Figure 5 illustrates the velocity streamlines of the fluid within the cyclone. It is evident that the air enters the system at a velocity of approximately 15 m/s and gradually decelerates as it approaches the outlets, exiting at around 7 m/s in both cases. Additionally, it can be observed that airflow predominates in the upper section of the cyclone, validating that the temperature is indeed higher in that region, as previously confirmed in Figure 4. The mass flow rate of particles does not significantly affect the fluid velocity, as the velocity profile remains similar for both cases. However, in the 16 g/s scenario, the velocity field becomes more chaotic due to the increased number of particles colliding with the fluid stream.

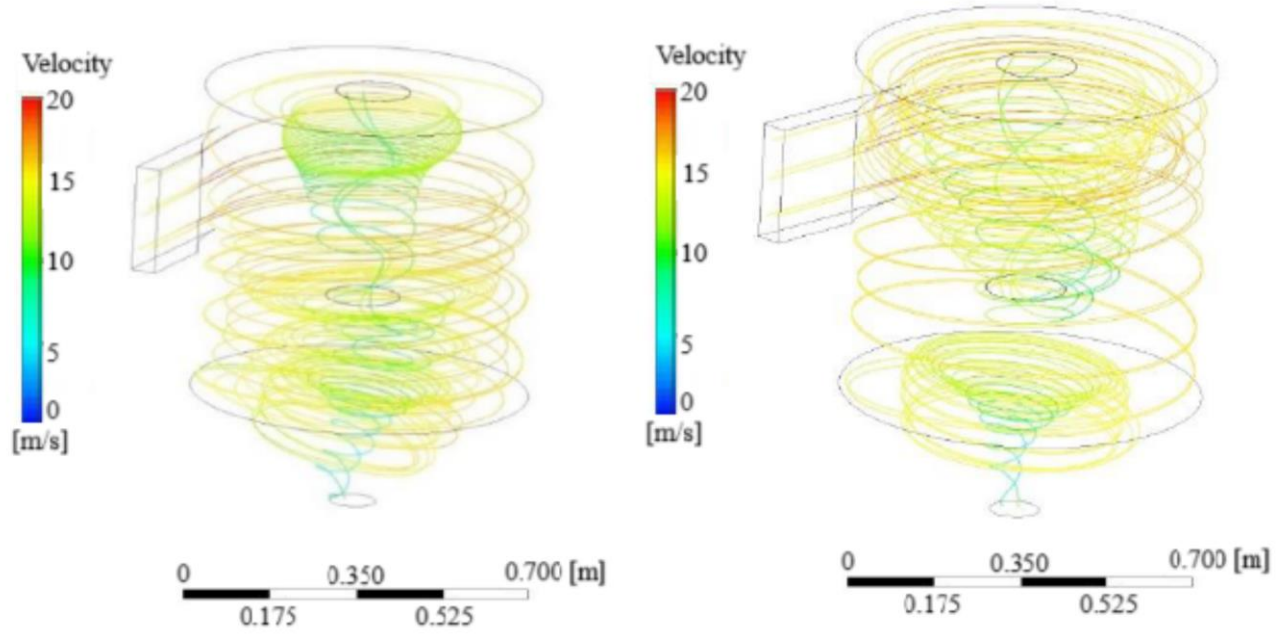

Figure 5. Fluid velocity streamlines for mass flow rates of 9.5 and 16 g/s, respectively.

Figure 6 illustrates the trajectory of a particle and its corresponding temperature variation within the cyclone. It is observed that the particle follows a natural path dictated by the internal flow field and exits through the bottom outlet. In both cases, the particle enters the cyclone at the same initial temperature of 30.6 °C, as detailed in Tab. 1. However, the final temperatures differ: 68 °C for the case with a mass flow rate of 9.5 g/s, and 63 °C for 16 g/s. This result supports the conclusion that a higher mass flow rate leads to a lower overall internal temperature within the cyclone, thereby causing the particles to exit at a reduced final temperature.

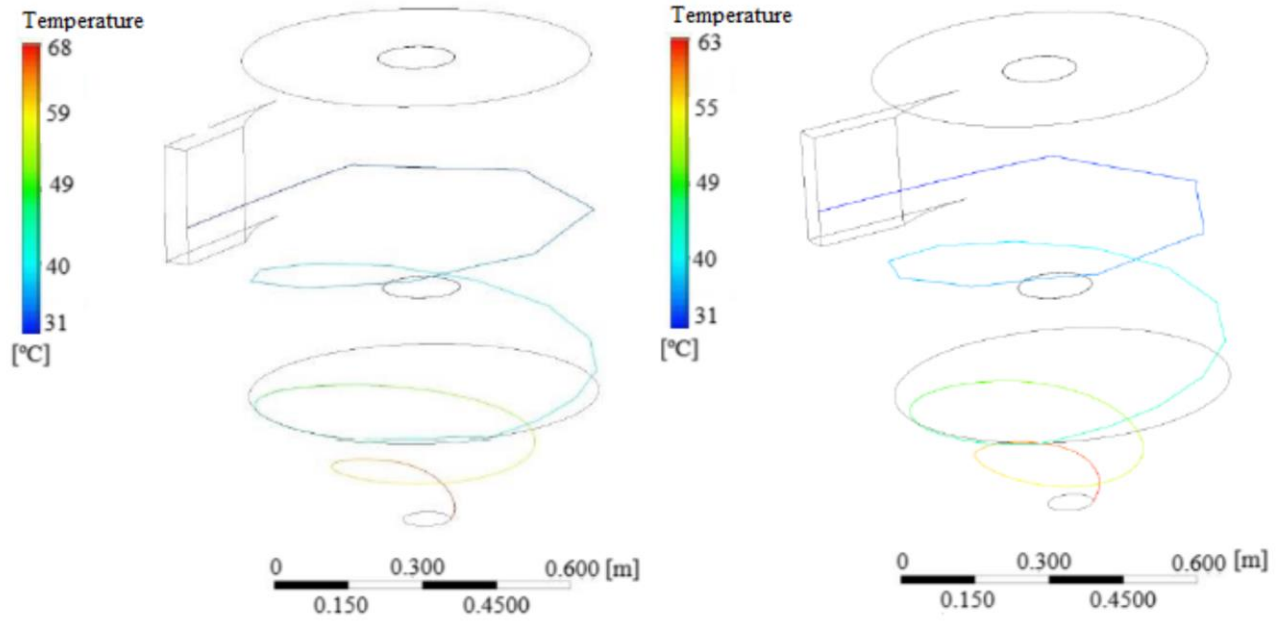

Figure 6. Particle trajectory and temperature during flow for mass flow rates of 9.5 and 16 g/s, respectively.

Figure 7 presents the pressure field within the cyclone. It can be observed that pressure decreases along the radial direction of the cyclone—from 509 Pa at the outer boundaries to a minimum of −148 Pa in the inner core for the 9.5 g/s case, and from 506 Pa to −175 Pa for the 16 g/s case. It is important to note that Figure 7 depicts the relative pressure distribution within the cyclone.

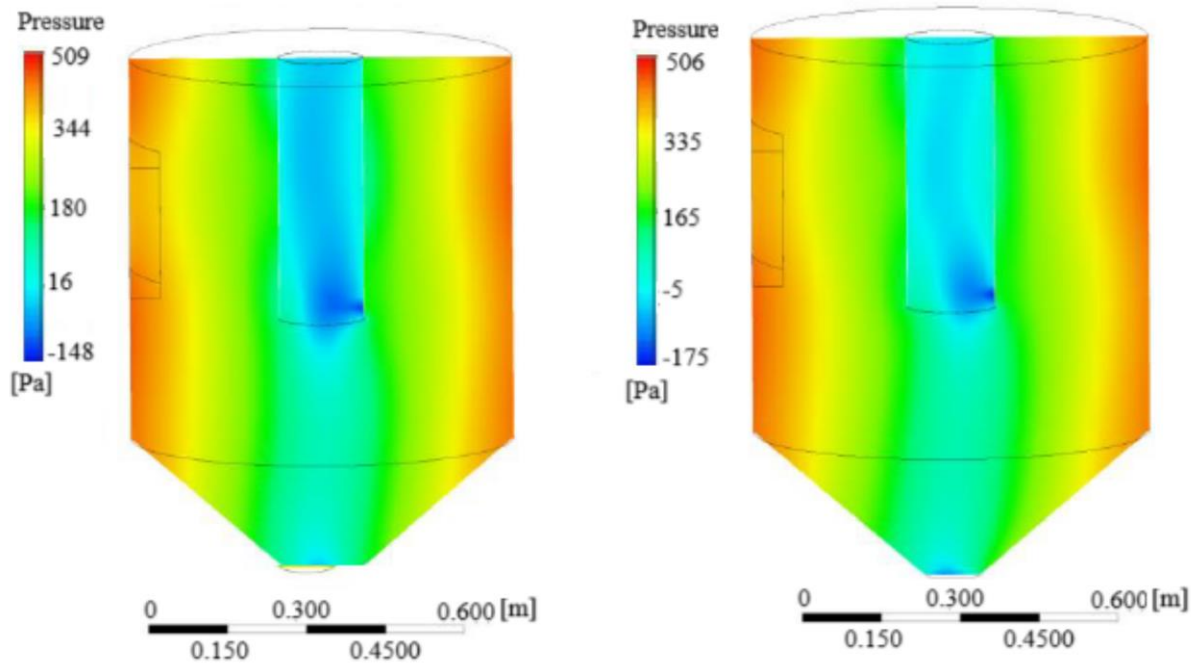

Figure 7. Internal pressure field of the cyclone for mass flow rates of 9.5 and 16 g/s, respectively.

4. CONCLUSION

This numerical study showed that increasing the particle mass flow rate from 9.5 g/s to 16 g/s significantly reduces the internal temperature of the cyclone, especially in the lower region, due to enhanced heat exchange between air and particles. However, the higher flow rate also leads to more chaotic airflow and lower exit temperatures for individual particles, reducing their heating efficiency. Despite the thermal gain from increased particle loading, the pressure becomes more negative in the cyclone core, and the process may lose efficiency if the flow rate is too low, as fewer particles are processed over time. Thus, an optimal balance between mass flow rate, internal temperature, and particle heating must be achieved. Future work should include transient analysis, geometry variations, and experimental validation to enhance model reliability.

5. REFERENCES

Azadi, M., Azadi, M. and Mohebbi, A., 2010. "A CFD study of the effect of cyclone size on its performance parameters". *Journal of Hazardous Materials*, Vol. 182, pp. 835–841. DOI: https://doi.org/10.1016/j.jhazmat.2010.06.115

Bahadori, A., Zahedi, G. and Zendehboudi, S., 2014. "Estimation of the effect of biomass moisture content on the direct combustion of sugarcane bagasse in boilers". *International Journal of Ambient Energy*, Vol. 35, No. 2, pp. 57–66. DOI: https://doi.org/10.1080/14786451.2012.748766

Brar, L. and Rahmani, F., 2024. "The impact of operating temperatures on the fluctuating flow field and precessing vortex core in cyclone separator using large-eddy simulations". *Physics of Fluids*, Vol. 36, No. 1, pp. 015101. DOI: https://doi.org/10.1063/5.0195382

Centeno-González, F.O., Lora, E.E.S., Nova, H.F.V. and Neto, L.J.M., 2017. "CFD modeling of combustion of sugarcane bagasse in an industrial boiler". *Fuel*, Vol. 194, pp. 274–285. DOI: https://doi.org/10.1016/j.fuel.2016.11.105

CONAB - *Companhia Nacional de Abastecimento, 2023. Acompanhamento da safra brasileira de cana-de-açúcar – primeiro levantamento (safra 2023/24) (in Portuguese)*. Brasília, DF, 11(1). ISSN: 2318-7921.

Corrêa, J. L. G., 2003. *Discussão de Parâmetros de Projeto de Secadores Ciclônicos (in Portuguese)*. Ph.d Thesis, Campinas Univesity, UNICAMP, Campinas, Brazil.

Dong, S., Jiang, Y., Jin, R., Dong, K. and Wang, B., 2020. "Numerical study of vortex eccentricity in a gas cyclone". *Applied Mathematical Modelling*, Vol. 80, pp. 683–701. DOI: https://doi.org/10.1016/j.apm.2019.11.024

Gupta, D., Gujre, N., Singha, S. and Mitra, S., 2022. "Role of existing and emerging technologies in advancing climate-smart agriculture through modeling: A review". *Ecological Informatics*, Vol. 71, pp. 101791. DOI: https://doi.org/10.1016/j.ecoinf.2022.101805

He, W., Yang, J. and Sun, G., 2025. "Inserting an Additional Vortex Finder to Improve the Performance of Cyclones in Series". *Separations*, Vol. 12, No. 3, pp. 60. DOI: https://doi.org/10.3390/separations12030060

Pérez, N.P., Machin, E.B., Pedroso, D.T. and Antunes, J.S., 2014. "Fluid-dynamic assessment of sugarcane bagasse to use as feedstock in bubbling fluidized bed gasifiers". *Applied Thermal Engineering*, Vol. 70, No. 1, pp. 994–1001. DOI: https://doi.org/10.1016/j.applthermaleng.2014.07.048

Safikhani, H., Rafiee, M. and Ashtiani, D., 2021. "Numerical study of flow field in new design cyclones with different wall temperature profiles: Comparison with conventional ones". *Advanced Powder Technology*, Vol. 32, pp. 3268–3277. DOI: https://doi.org/10.1016/j.apt.2021.07.017

Siadaty, M., Kheradmand, S. and Ghadiri, F., 2017. "Study of inlet temperature effect on single and double inlets cyclone performance". *Advanced Powder Technology*, Vol. 28, pp. 1459–1473. DOI: https://doi.org/10.1016/j.apt.2017.03.015

Silva, J. P. P. A, 2016. *Secador Ciclônico: Modelagem e Simulação Via CFX (in Portuguese)*. Master's thesis, Federal University of Campina Grande, Campina Grande, Brazil.

Yohana, E., Tauviqirrahman, M., Laksono, D., Charles, H., Choi, K. and Yulianto, M., 2022. "Innovation of vortex finder geometry (tapered in-cylinder out) and additional cooling of body cyclone on velocity flow field, performance, and heat transfer of cyclone separator". *Powder Technology*, Vol. 410, pp. 117235. DOI: https://doi.org/10.1016/j.powtec.2022.117235

Yuan, S., Sun, G., Cao, G., Habudula, G. and Liu, J., 2024. "Numerical calculation on the short-circuit flow rate in a gas cyclone". *Chemical Engineering Research and Design*, Vol. 205, pp. 177–187. DOI: https://doi.org/10.1016/j.cherd.2024.05.032

5. RESPONSIBILITY NOTICE

The author(s) is (are) the only responsible for the printed material included in this paper.